Self-organized ZnO nanofractal array

Pradosh K. Sahoo, G. Mangamma*, M. Kamruddin, S. Dash, Ashok K. Tyagi

Surface and Nanoscience Division, Material Science Group, Indira Gandhi Centre for Atomic Research, Kalpakkam, 603102, India

*Corresponding author; Tel: (044) 27480500, Ext.-22232; E-mail: gm@igcar.gov.in

Received: 08 April 2016, Revised: 15 October 2016 and Accepted: 05 November 2016

DOI: 10.5185/amp.2017/839
www.vbripress.com/amp

Abstract

In the present work ZnO dendritic nanostructures (NS) were synthesized by sol-gel and spin coating methods over silicon (100) substrate. The phase purity was confirmed by XRD. Grain size was found to be less than 10 nm. The vibrational modes of the nano ZnO wurtzite structure were observed by laser Raman spectroscopy. Raman spectra revealed asymmetrically broadened red shift of E_2 (high) optical phonon mode which accrues from contribution of Non-Brillouin Zone (NBZ) phonons. The shift in the peak is attributed to the quantum mechanical confinement of phonon due to their nano grains as inferred from XRD and morphological studies by Scanning Electron Microscopy (SEM) and Atomic Force Microscopy (AFM). SEM and AFM images revealed the leaf like dendrite structures having several branches. Possible growth mechanism has been discussed in line with the synthesis. Box counting method was implemented to determine the fractal dimension (D) and the value of D is found to be ~1.6±0.1. This work will be useful in designing novel optoelectronic devices and sensors from ZnO nanostructures (NS) exhibiting complex morphology.

Keywords: ZnO, nano, fractal, AFM, self-organization.

Introduction

ZnO has been a material of high research interest during the recent past due to its remarkable properties of being a direct wide band gap (3.37 eV) semiconductor, high exciton binding energy (60 meV) **[1]**, photocatalytic activity **[2, 10**], piezoelectricity **[3]** as well as high environmental and chemical stability **[4]**. It exhibits several morphologies at nanoscale such as nanoparticles **[5]**, nano wires **[6**], nanorods **[7]**, nanocombs, nanobelts, nanohelixes **[8]**, nanoflowers **[9]**, fern like nanoleaves **[10]** and nanotetrapods **[11**]. Based on morphological structures the properties of ZnO NS differ from one case to another **[12]**. Therefore, in the current years morphology dependent studies of materials have been an active research area **[13]**. In 2005, R. Wu etal has synthesized ZnO tetrapod nanowhiskers by thermal evaporation of Zn vapor in presence of Ar and O_2 mixture. They calculated the fractal dimension of the whiskers to 1.7 and reported, well developed crystalline feet and enhanced optical properties obtained through photoluminescence spectroscopy **[14]**. In 2015, fern like ZnO nanoleaves were obtained by Q. L. Ma et al by ultrasonicating zinc microcrystals in water. It exhibited four times better photocatalytic property than spherical ZnO nanoparticles **[10**]. There are also several reports available in literature on enhanced physical and chemical properties of ZnO due to its complex morphology which is not mentioned here.

Therefore, we have synthesized ZnO NS with fractal architecture which can exhibit enhanced optical properties and photocatalytic activity. Such dendritic ZnO nanostructures (NS) will be useful in the fabrication of novel nano optoelectronics devices due to enhanced optical property. In addition, such structures exhibit improved photocatalytic activity which can be implemented for energy harvesting, solar cells as well as chemical sensors. Also, a possible growth mechanism has been suggested for the formation of such complex dendritic structures. The morphology of the ZnO NS brought about in the current study is unique compared to other morphologies of ZnO reported in the literature in its shape with reduced size. Further studies on its mechanical and piezoelectric properties are going on for its viability for different electronics and optoelectronics applications.

Materials and methods

ZnO dendritic NS were synthesized through sol-gel and spin coating methods. The chemicals used in the synthesis are Zincacetate dehydrate (ZAD), isopropanol (2-Propanol) and monoethanolamine (MEA) as precursor, solvent and surfactant respectively. All the chemicals were purchased from Merck Company (Germany) with 99.9 % purity and used without further purification. First ZAD was added to isopropanol and stirred for 1 hour resulting a milky solution. Then suitable amount of MEA was added maintaining the molarity of the solution 0.5 moles/liter and stirred for another 1 hour. It resulted a

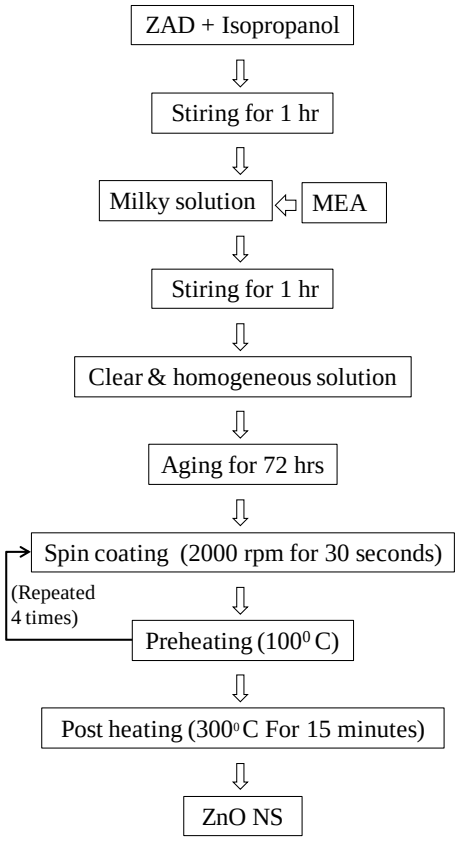

Fig. 1. Schematic of synthesis procedure.

transparent homogeneous solution. This solution was spun at 2000 revolutions per minute for 30 seconds after putting it over Si (100) substrates after 72 hours of aging. Prior to spin coating, the Si substrates were cleaned using acetone, isopropanol and deionized water. After performing the spin coating for five times heat treatment was provided in a furnace at 300^0 C for 15 minutes under ambient condition with 100^0 C prior heat treatment after each coating. A schematic diagram of the synthesis procedure is represented in **Fig. 1**.

As per the proposed sol gel mechanism, ZAD would transfer to zinc monoacetate, $[CH_3COOZn]^+$ after it was added to isopropanol **[15]**. Then $[CH_3COOZn]^+$ forms a complex with MEA in the course of process which is described below.

$$Zn(CH_3COO)_2 \longrightarrow [CH_3COOZn]^+ + [CH_3COO]^-$$

$$HO{-}CH_2CH_2{-}NH_2 + [CH_3COOZn]^+ \longrightarrow HO{-}CH_2CH_2{-}NH_2{-}Zn{-}O{-}\overset{\overset{O}{\|}}{C}{-}CH_3$$

The above reactions will lead to hydrolysis and dehydration polycondensation for which the reaction steps are written below.

$$HO{-}CH_2CH_2{-}NH_2{-}Zn{-}O{-}\overset{\overset{O}{\|}}{C}{-}CH_3 + H_2O \longrightarrow HO{-}CH_2CH_2{-}NH_2{-}Zn{-}O{-}H + CH_3COOH$$

$$HO{-}CH_2CH_2{-}NH_2{-}Zn{-}O{-}H \quad H{-}O{-}Zn{-}NH_2{-}CH_2CH_2{-}OH \longrightarrow HO{-}CH_2CH_2{-}NH_2{-}Zn{-}O{-}Zn{-}NH_2{-}CH_2CH_2{-}OH + H_2O$$

The complex oligomers $Zn_2O(NH_2CH_2CH_2OH)_2$ will lead to the formation of ZnO after the final heat treatment.

All the measurements were performed at room temperature ((~20^0 C) and in a less humidity (<50 %) atmosphere. The structural characterization was carried out by XRD (STOE, Cu Kα). The vibrational modes of wurtzite ZnO were studied by a Raman spectrometer (Renishaw invia Raman Microscope, UK) with laser wavelength 514 nm and spot size 1 µm diameter. The morphology of the structures was studied by SEM (AURIGA Cross beam, ZEISS, Germany) and AFM (NTEGRA, NTMDT, Russia).

Results and discussion

XRD

Fig. 2 shows the XRD pattern for the ZnO NS with fractal architecture. It represents that the material is nanocrystalline in nature with good crystalline quality. The peaks present in the XRD pattern match well with the JCPDS data (powder diffraction, card no: 36-1451) of ZnO having hexagonal wurtzite structure with lattice parameters a=3.24982 A^0 and c=5.20661 A^0. The average crystallite size was calculated using the Scherrer equation which is given by,

$$D = \frac{0.9\lambda}{\beta \cos\theta} \quad (1)$$

where, D is the average crystallite size, λ (1.5406 A^0) is the wave length of X-ray used, β is the full width at half maximum (FWHM) and θ is the Bragg angle.

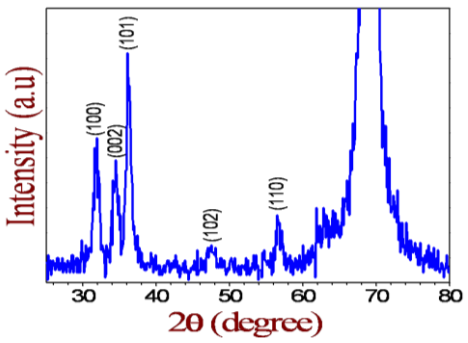

Fig. 2. XRD pattern of ZnO NS.

Table 1. Typical values for crystallite size obtained from XRD of ns ZnO.

Plane (hkl)	Crystallite size (nm)
100	9
002	9
101	10

The crystallite size obtained from broadening of (100), (002), (101) planes are listed in **Table 1**.The average crystallite size as obtained from peak broadening is found to be ~10 nm.

The lattice parameters, a and c have also been calculated by using the equations (2) and (3) and found to be 3.243 A^0 and 5.199 A^0 respectively.

$$a = \frac{\lambda}{\sqrt{3}\sin\theta} \quad (2)$$

$$c = \frac{\lambda}{\sin\theta} \quad (3)$$

A comparison of our calculated lattice constants with the bulk ZnO provides a good agreement. Therefore **Fig. 2** has confirmed that ZnO nanofractals with hexagonal wurtzite structure are resulted through sol-gel and spin coating process.

Raman spectroscopy

The vibrational modes of the ZnO dendritic NS were studied through Laser Raman spectroscopy. Fig .3 shows the Raman spectra of NS ZnO. ZnO has the hexagonal wurtzite structure and belongs to C^4_{6V} ($P6_3mc$) space group. According to the prediction of group theory, ZnO exhibits eight sets of phonon modes: $2E_2$, $2A_1$, $2E_1$ and $2B_1$. Among them, the $2B_1$ modes are Raman silent **[16]**. Raman spectra from various regions (spot-1 to 4) of the film in **Fig. 3** depict the two prominent peaks at 99 cm^{-1} and 435 cm^{-1}. The first peak at 99 cm^{-1} (E_2 low), dominated by the vibrations of the heavy Zn sublattice. The second material peak is at 435 cm^{-1} (E_2 high) which involves mostly the oxygen atoms. The zinc and oxygen ions move perpendicular to the c-axis and opposite to each other. Therefore, the displacements of the ions sum up to zero, resulting net polarization zero. Further, A_1 and E_1 phonons are oxygen-dominated polar modes. The ions either move parallel or perpendicular to the c axis, corresponding to A_1 and E_1 symmetries respectively in such a way that the displacement of the Zn sub lattice with respect to the oxygen sublattice induces a net oscillating polarization.

The Raman active modes of bulk ZnO for E_2 high and E_2 low are 439 cm^{-1} and 102 cm^{-1} respectively **[17]**. These main observed peaks at 435 cm^{-1} and 99 cm^{-1} are close to the Raman active modes of bulk ZnO. Particularly the E_2 high is a strong mode and it is considered as the signature of ZnO wurtzite structure.

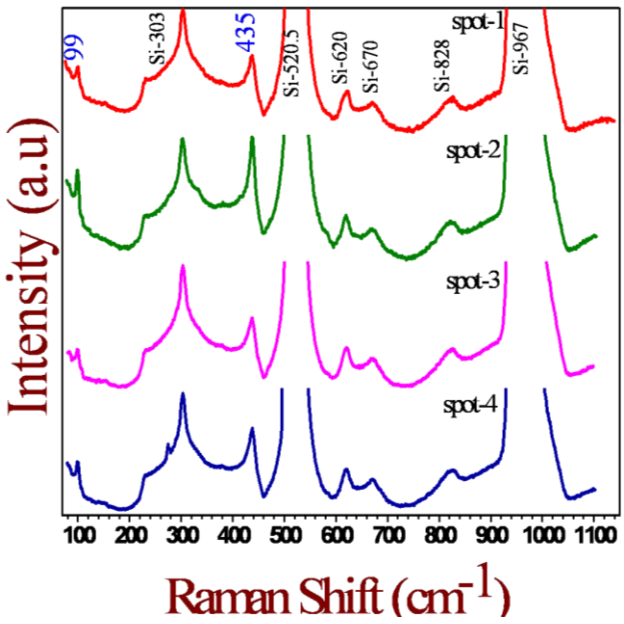

Fig. 3. Raman spectra of ZnO NS.

Table 2. Raman peaks positions and their relative shifts of NS wurtzite ZnO.

ZnO	Spots	E_2 High (cm^{-1})	Δω, E_2 High (cm^{-1})	E_2 low (cm^{-1})	Δω, E_2 low (cm^{-1})
Bulk		439		102	
Nano	1	435	4	99	3
	2	436.5	2.5	99	3
	3	435	4	98	4
	4	435	4	99	3

As shown in **Table 2**, the peak positions depicted in **Fig. 3** are red shifted by 4 cm^{-1} and 3 cm^{-1} in comparison to the peak positions of bulk ZnO. Such shifts can be attributed to optical phonon confinement in nanostructures. In other words, there are two possible mechanisms for the phonon peak shifts in Raman spectra of ZnO nanostructures. 1. Spatial confinement within the nanocrystal boundaries of quantum dot architecture **[17]**. 2. Phonon localization by defects. Nanocrystals or quantum dots, produced by chemical methods, generally have more defects than corresponding bulk counterparts. Several reports on the spatial confinement of optical phonons have been reported in literature **[18, 20]**. In each case, it is established that Raman spectra of nanocrystalline semiconductors red shift and broaden due to relaxation of the selection rule in the finite size nanocrystals. Due to the optical anisotropy of wurtzite lattice, optical-phonon confinement in wurtzite nanocrystals leads to distinctively identifiable changes in Raman spectra.

SEM

Figs. 4 (a) and **(b)** show SEM micrographs of ZnO nanofractal array with lower and higher magnification. It represents formation of leaf like dendritic structures having several branches. The branching effect is attributed to the self-organization of individual structures during the growth process necessitating minimization of surface energy. Length of the branches varies in the range of 1 to 10 µm and width of the branches is ~100 nm. Formation mechanism of the fractal nanostructure depends on growth rate, concentration of oxygen, cooling rate and also diffusion length as well as rate of atomic diffusion across island edges. Response of such fractal landscape to applied field will be novelty which will explain piezoresponse in a unique way.

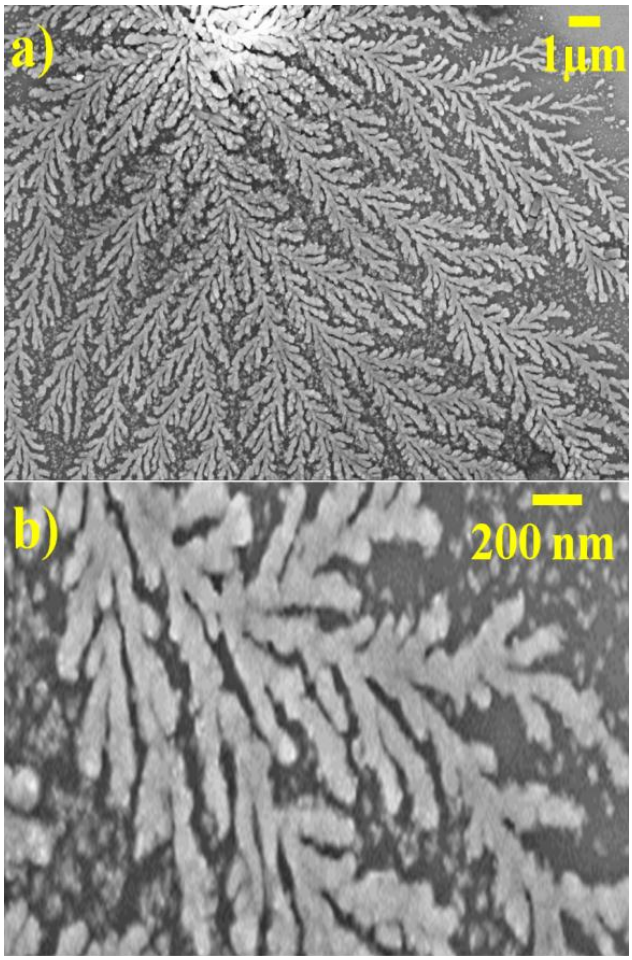

Fig. 4. SEM micrographs of ZnO dendritic NS (a) low magnification (b) high magnification.

AFM

Fig. 5 shows the topography of the ZnO NS studied through AFM in noncontact mode. **Figs. 5 (a), (b)** and **(c), (d)** represent the 2-dimensional (2-D) and their corresponding 3-dimensional (3-D) topographic images for large and small area scan. Large area images provide

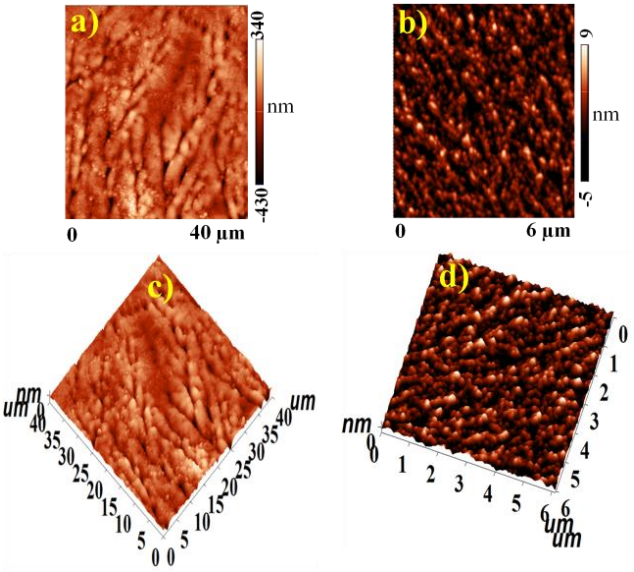

Fig. 5. AFM micrographs of ZnO dendritic NS (a), (b) 2-D topographic images of large and small area scan and (c), (d) corresponding 3-D topographic images respectively.

uniform distribution of the nano structures whereas small area images give an idea about the formation of nano fractal assembly during growth process. This also provides the confirmation of the patterns observed in various regions. The length of the branches varies in the range 1 to 13 µm and width is of the order of 90 nm. Both AFM and SEM micrographs show identical patterns. A careful observation of identical micrographs acquired in two different length scales establishes formation of such scale invariant fractal assemblies.

Growth mechanism

Here we provide a possible mechanism for the growth of such complex patterns. The formation of the structures in a polycrystalline material comes from the preferential growth of several planes. Here XRD reveals peaks corresponding to five planes of wurtzite ZnO in **Fig. 2**, out of which (100), (002) and (101) are prominent. Though there is a fixed angle between different planes of ZnO, SEM micrograph presented in figure-4 does not reveal any fixed angle between main branches and sub branches. This implies that the growth of the dendritic structures is significantly dominated by ZnO precursors through self-organization rather than preferential growth due to various planes.

One can tune the ZnO nanostructures by careful adjustment of the temperature, vapour pressure and oxygen partial pressure. The growth process for the nanofractals is even more complex. If the concentration is kept at a certain value, the growth can proceed in a thermodynamic equilibrium state. But fractal growth may arise from the nonequillibrium thermodynamic state leading to the petal like structures. This may be due to the formation of multiple nuclei in the primary stage than that for nanorods and particles. As shown in SEM and AFM

images, the formation of multiple nuclei arises due to the coexistence of enormous number of facets. Hence such a structure is possible with sufficient high energy for multiple stem formation. As a result, complex growth process for the nanofractal occurs. Actual mechanism is nevertheless to be investigated. In general, the growth mechanism of the wire and multiple twigs-like nanostructures could be explained by the kinetics of anisotropic growth mechanism. The two-dimensional nucleation probability, P on the surface of nanostructures with a surface energy, σ at temperature, T is given by

$$P=B \exp [-\pi\sigma^2/ (K_BT)^2 \ln\alpha] \quad (4)$$

where, α (>1, usually) is the supersaturation ratio between the actual vapor pressure and the equilibrium vapor pressure corresponding to temperature, B is the parameter constant and K_B is the Boltzmann's constant.

The supersaturation ratio is a convenient growth parameter. This can ascertain the morphology of the material. Under high supersaturation ratio conditions, the growth results in a multiple twig like structure. Whereas the growth under a low supersaturation ratio condition results in nano wire-like structures, So the higher supersaturation ratio of ZnO dendritic NS could be correlated to the dense packed structures in films or the higher deposition rate.

Fractal dimension

The fractal dimension of a structure determines its geometric complexity. To determine the fractal dimension of the ZnO dendrite structures, the popular box counting method has been implemented. This was executed by inserting square grids to the SEM image (**Fig. 4**) through imagej software. The standard formula for determining fractal dimension, D is given by,

$$D = \frac{\log N(\epsilon)}{\log 1/\epsilon} \quad (5)$$

where Є is the scale factor and N (Є) is the number of occupied boxes by the fractal structure.

The fractal dimension calculated here for this complex pattern is ~1.6±0.1. This value is in good agreement with the fractal dimension of other ZnO fractal architectures with complex morphology exhibiting enhanced optical and photocatalytic properties. Therefore, it provides a high possibility in the enhancement of physical and chemical properties which may lead to the fabrication of integrated electronic devices and sensors at nanoscale with large efficiency.

Conclusion

ZnO dendritic NS have been synthesized successfully by sol gel and spin coating method. The crystal structure of wurtzite ZnO NS has been confirmed by XRD and Raman Spectroscopy. The average crystallite size is ~10 nm as calculated form XRD. Analysis of Raman data clearly revealed quantum mechanical confinement of phonons due to nanostructures. SEM and AFM have revealed similar patterns of nanofractal array showing the formation and stability of the material. The length and width of the stem constituting the fractals are about 1 to 13 µm and ~100 nm respectively. The growth mechanism is discussed considering two fundamental competing parameters and concluded that the formation of such complex patterns is subjugated by the self-organization of ZnO precursors rather than the preferential growth. In addition, it is explained in terms of the non-equilibrium of thermodynamic steady state leading formation of entropy minimized assemblies. This may be due to the formation of multiple nuclei. Multiple nuclei accommodation coupled to fast atomic diffusion across nuclei interfaces can be a contributing factor behind the genesis of fractal architectures. The value of fractal dimension calculated by box counting method and is ~1.6±0.1. Further improvement in the shape and size of such complex structures can be made by the optimizing solution concentration, aging time, spin speed as well as duration of spinning and heat treatment. Such nanofractal architectures of ZnO would exhibit enhanced performance of nanodevice in comparison to those based on nanoparticles, nanorods, nanowires, etc.

Acknowledgements

The authors are thankful to department of atomic energy for providing the financial aid to carry out this work. The authors would also like to wish their gratitude Dr. S. Kalavathy Mr. S. R. Polaki and Dr. A.Rajesh for their constant help and support.

Author's contributions

Conceived the plan: Dr.G. Mangamma and P. K. Sahoo; Performed the expeirments: P. K. Sahoo; Data analysis: P. K. Sahoo and Dr. G. Mangamma ; Wrote the paper: pks, gm. Review: mk, sd and akt. Authors have no competing financial interests.

Supporting Information

Supporting informations are available from VBRI Press.

References

1. That, C.; Weston, L.; Philips, M. R.; *Phys. Rev. B*, **2012,** *86*, 115205. **DOI**: 10.1103/PhysRevB.86.115205
2. Wan, Q.; Wang, T. H.; Zhao, J. C.; *Appl. Phys. Lett.*, **2005**, *87*, 083105. **DOI:** 10.1063/1.2034092
3. Saini, D.; Dickel, D.; Podila, R.; Skove, M. J.; Serkiz, S.; Rao, A. M.; *Phys. Rev. B*, **2012**, *86*, 205312. **DOI**: 10.1103/PhysRevB.86.205312
4. Radzimska, A. K.; Jesionowski, T.; *Materials*, **2014**, *7*, 2833. **DOI**: 10.3390/ma7042833
5. Sondergaard, M.; Bojesen, E. D.; Christensen, M.; Iversen, B. B.; *Cryst. Growth Des.*, **2011**, *11*, 4027. **DOI**: org/10.1021/cg200596c
6. Jean, J.; Chang, S.; Brown, P. R.; Cheng, J. J.; Rekemeyer, P. H.; Bawendi, M. G.; Gradec, S.; Bulovic V.; *Adv. Mater.*, **2013**, *25*, 2790. **DOI**: 10.1002/adma.201204192
7. Schlur, L.; Carton, A.; Leveque, P.; Guillon, D.; Pourroy, G.; *J. Phys. Chem. C*, **2013**, *117*, 2993. **DOI**: org/10.1021/jp305787rl

8. Wang, Z. L.; J. *Phys.: Condens. Matter*, **2004,** *16*, R829.
DOI: 10.1088/0953-8984/16/25/R01
9. Hsueh, H. T.; Chen, Y. H.; Lin, Y. D.; Lai, K. C.; Chen, J. W.; Wu, C. L.; *Appl. Phys. Lett*., **2013,** *103*, 213109.
DOI: org/10.1063/1.4832485
10. Ma, Q. L.; Xiong, R.; Zhai, B.; Huang, Y. M.; *Appl. Surf. Sci*., **2015**, *324*, 842.
DOI: Not available
11. Gedamu, D.; Paulowicz, I.; Kaps, S.; Lupan, O.; Wille, S.; Haidarschin, G.; Mishar, Y. K.; Adelung, R.; *Adv. Mater*., **2014**, *26*, 1541.
DOI: 10.1002/adma.201304363
12. Sun, X. W.; Yang, Y.; ZnO Nanostructures and Their Application; CRC Press: USA, **2012**.
ISBN: 13: 978-9-81430-391-0
13. Zhang, S.; Nanostructured Thin films and Coatings; CRC Press: USA, **2010**.
ISBN: 978-1-4200-9395-7
14. Wu, R.; Yang,, Y.; Cong, S.; Wu, Z.; Xie, C.; Usui, H.; Kawaguchi, K; Koshizaki, N.; *Chem. Phys. Lett.*, **2005**, *406*, 457.
DOI: 10.1016/j.cplett.2005.03.030
15. Wang, M.; Wang, J.; Chen, W.; Cui, Y.; Wang, L.; *Mater. Chem. Phys.*, **2006**, *97*, 219.
DOI: 10.1016/j.matchemphys.2005.07.072
16. Decremps, F.; Porres, J.P.; Saitta, A. M.; Chervin, J. C.; Polian, A.; *Phys. Rev. B*, **2001**, *65*, 092101.
DOI: 10.1103/PhysRevB.65.092101
17. Khan, A. A.; Vladimir, A. F.; Manu, S.; Alexander, A. B.; *J. Appl. Phys.*, **2005,** *97*, 124313.
DOI: 10.1063/1.1944222
18. Lin, K. F.; Cheng, H. M.; Hsu, H. C.; Hsieh, W. F. *Appl. Phys. Lett*., **2006,** *88*, 263117.
DOI: 10.1063/1.2218775
19. Khan, A. A.; Vladimir, A. F.; Alexander, A. B.; *Appl. Phys. Lett*., **2005**, *86*, 053103.
DOI: 10.1063/1.1861509
20 Rajalakshmi, M.; Arora, A. K.; Bendre, B. S.; Mahamuni, S.; *Appl. Phys. Lett*., **2000**, *87*, 5.
DOI: 10.1063/1.372199

